Organic Depth Profiling
With the PHI Model 06-C60 Sputter Ion Gun

Introduction: Physical Electronics introduced the model *06-C60* C_{60} sputter ion gun and its unique capabilities for surface cleaning and depth profiling of soft materials (figure 1) to the XPS community in 2004.[1] Since that time more than sixty model *06-C60* ion guns have been installed in laboratories around the world and C_{60} cluster source depth profiling of soft materials has become an established and exciting new capability for XPS practitioners.[1,2,3]
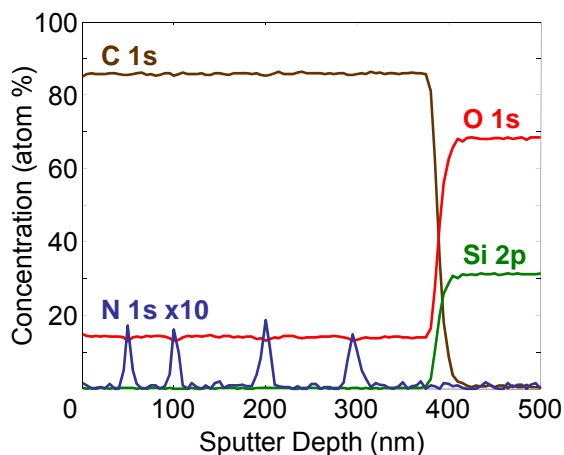

Figure 1. 10 kV C_{60}^+ sputter depth profile of 3 nm Irganox 3114 layers in an Irganox 3110 film.

The *06-C60* produces a 10 kV mass filtered C_{60} ion beam. Upon impact with the sample, the large C_{60} cluster releases its energy in the near surface region providing a highly efficient sputtering process that exposes a subsurface layer that has sustained minimal chemical damage.[4] In contrast, monatomic ion sources such as Ga^+ and Ar^+ sputter inefficiently and individual ions can penetrate below the surface causing chemical damage in and beyond newly exposed subsurface layers. Shown in figures 2 and 3 are pictorial models of the sputtering processes for C_{60}^+ and Ga^+ impacting a surface at normal incidence.[4]

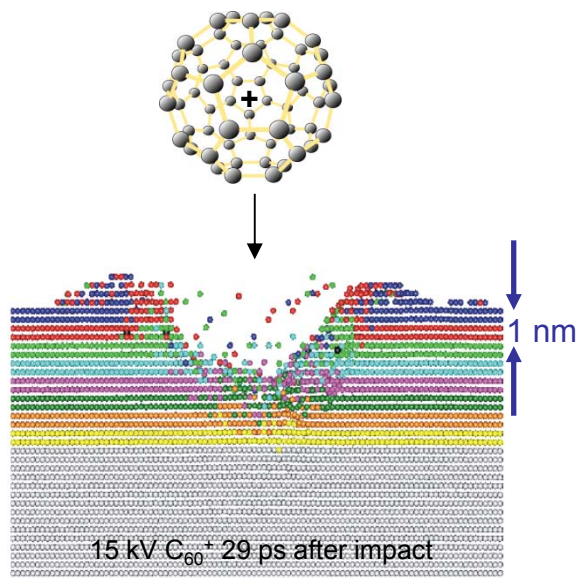15 kV C_{60}^+ 29 ps after impact

Figure 2. Ion impact simulations show that a C_{60} ion very efficiently removes material in the surface region, does not penetrate into the material, and exposes a relatively undamaged subsurface layer for analysis.[4]
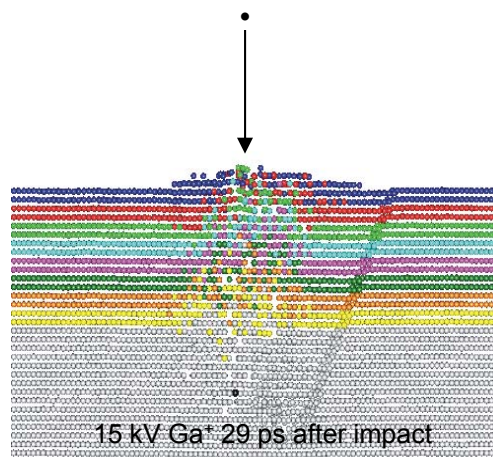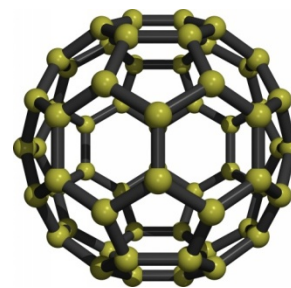

15 kV Ga^+ 29 ps after impact

Figure 3. Ion impact simulations show that a monatomic ion such as Ga^+ or Ar^+ is not very efficient at removing material, penetrates into the material, and is likely to create chemical damage in the subsurface region exposed for analysis.[4]
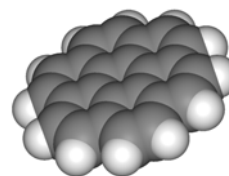
Why C_{60}? The growing importance of organic and polymer films for the construction of advanced materials and devices has created a need for the ability to characterize these thin film structures. It is well known that monatomic Ar^+ sputtering, even with a low accelerating voltage, causes major chemical damage to organic and polymer surfaces, limiting its usefulness for XPS thin film analysis of organic and polymer materials. Cluster ion sources however, have been shown to be useful for the characterization of these films by XPS depth profiling.

The composition, mass, and shape of the cluster ion appears to be of critical importance to the ability to depth profile polymers and organics and obtain meaningful chemical information. As shown in figures 2 and 3, a large cluster ion such as C_{60}^+ has a shallow penetration depth compared to a single atom ion source. Because of its large spherical shape C_{60} ions cannot penetrate a significant distance into the material it impacts. As a result, on impact the C_{60} ion is believed to collapse and impart its momentum to atoms in the surface region resulting in high sputtering efficiency. The results of the C_{60} sputtering process are a shallow penetration depth, efficient sputtering, and the creation of a very thin damage layer. It has been shown that an instrument configuration that delivers the C_{60} ions at a shallow angle relative to the sample surface optimizes the desirable characteristics of C_{60} sputtering for chemical depth profiling.[5]

Coronene is a disk shaped cluster with half the mass of C_{60}. In contrast to C_{60} which is chemically inert in most polymers, coronene contains a significant amount of H that when ionized may chemically interact with some polymers. Coronene has been successfully applied to polymers with O and F linkages. However, just as it is easy to understand why monatomic Ar^+ is of almost no value for sputtering organics and polymers, it is reasonable to assume that there may be materials that will not work with coronene but will work with C_{60} because of the difference in the composition, mass, and shape of the cluster ion.

C_{60} – 720 amu
Buckminster Fullerene

$C_{24}H_{12}$ – 300 amu
Coronene

Ar – 40 amu

Figure 4. Common ions used today for XPS sputter depth profiling.

Figure 5. PHI model 06-C60 Ion Gun.

From a practical view point it has been demonstrated by PHI that C_{60} ion sources can be manufactured at a reasonable cost and maintained to provide stable etch rates and long source lifetimes. Today more than sixty PHI model *06-C60* ion guns have been installed around the world.

C_{60}^+ vs. Ar$^+$: Ar$^+$ sputtering has a been successfully applied to the study of inorganic materials and thin films for many years. However, for most organics and polymers monatomic Ar$^+$ sputtering is known to cause severe chemical damage. Even low voltage (≤ 250 V) Ar$^+$ sputtering has very limited success for organics and polymers.

In sharp contrast to Ar$^+$, C_{60}^+ sputtering has been shown to preserve chemistry and composition when depth profiling a number of commonly used organics and polymers that contain O and F linkages (PET, PMMA, PTFE, etc).[6]

To illustrate the difference between C_{60}^+ and Ar$^+$ sputtering for organics and polymers, sputter depth profiles were obtained from a 100 nm thick film of PMMA on a Si substrate and are shown in figures 6 and 7 on this page. This work was performed at room temperature.

The most visible difference between C_{60}^+ and Ar$^+$ sputtering of this PMMA sample is that the chemistry and composition is preserved throughout the PMMA film when sputtering with 10 kV C_{60}^+ and that with 250 V Ar$^+$ sputtering there is an immediate loss of O indicating severe chemical damage is taking place with 250 V Ar$^+$ sputtering.

Another observation from this data is how efficiently C_{60} sputters polymers such as PMMA as shown in figure 8. In this case, the etch rate for PMMA with 10 kV C_{60}^+ was 20X faster than the 0.4 nm/min etch rate for SiO_2 using these conditions. The etch rate for PMMA using 250 V Ar$^+$ was only 1.6X faster than the 0.3 nm/min etch rate for SiO_2 using these conditions.
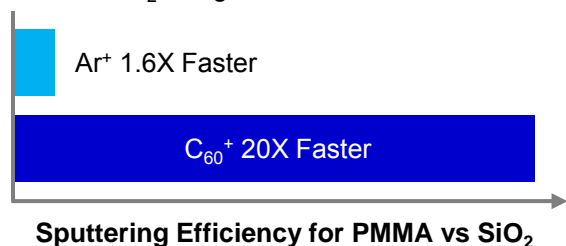
Ar$^+$ 1.6X Faster

C_{60}^+ 20X Faster

Sputtering Efficiency for PMMA vs SiO_2

Figure 8. C_{60} sputter etch rates are high for many commonly used industrial polymers.

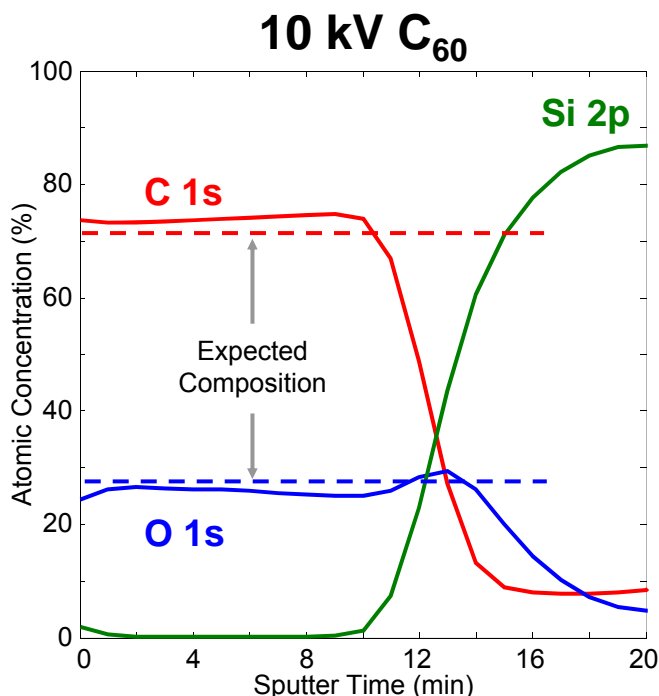# 100 nm PMMA Film on Si Wafer

10 kV C_{60}

Figure 6. 10 kV C_{60}^+ depth profile of a 100 nm thick PMMA film on a Si wafer substrate showing the preservation of chemical composition as a function of depth with C_{60} sputtering.
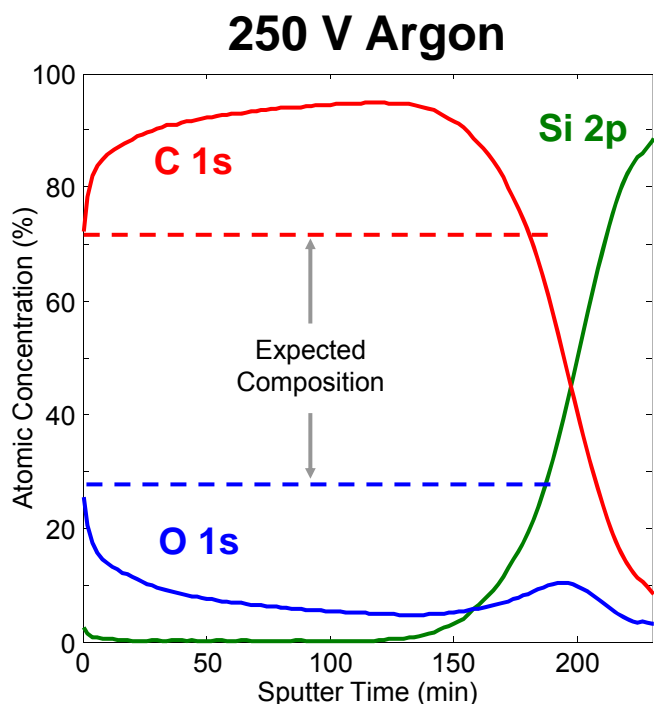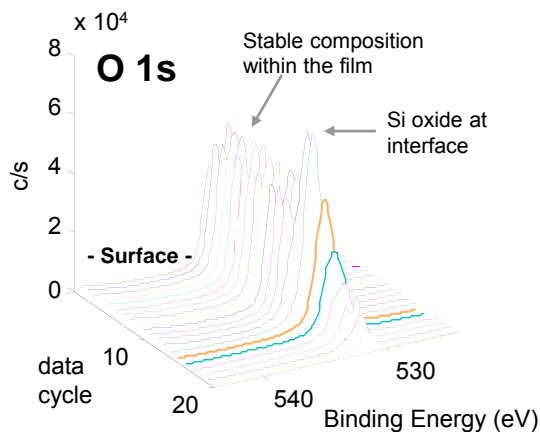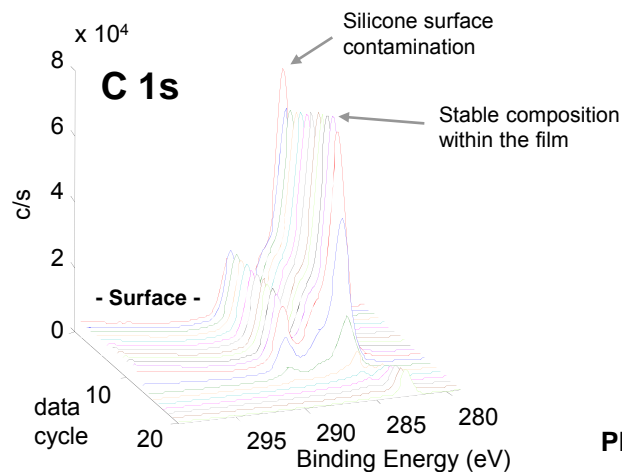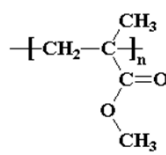
250 V Argon

Figure 7. 250 V Ar$^+$ depth profile of a 100 nm thick PMMA film on a Si wafer substrate showing immediate and severe chemical damage even with a very low energy Ar ion beam.

100 nm PMMA Film
10 kV C_{60}^+ Depth Profile

100 nm PMMA Film
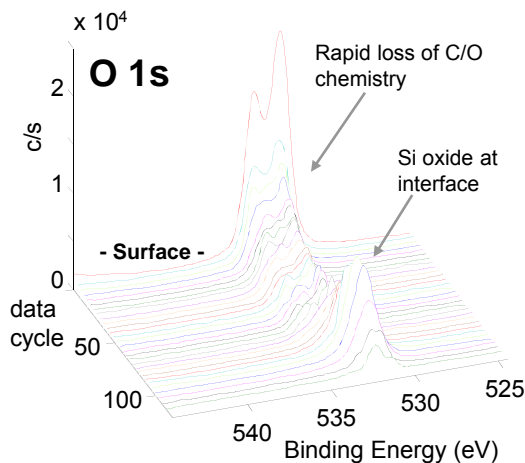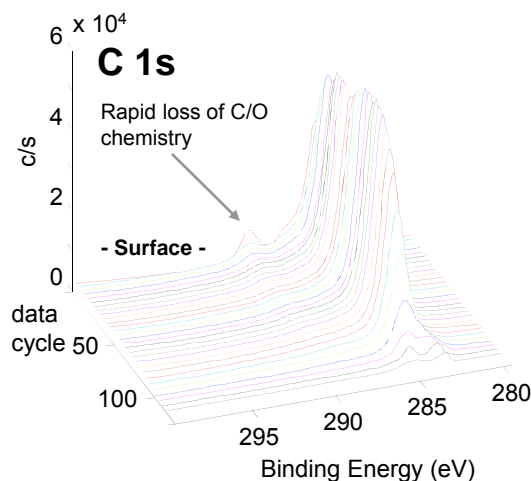# 250 V Ar^+ Depth Profile

PMMA

Figure 9. Montage plots of the individual spectra from the 10 kV C_{60}^+ depth profile show the ability to provide meaningful chemical information throughout the profile.

Figure 10. Montage plots of the individual spectra from the 250 V Ar^+ depth profile show rapid and significant chemical damage that limits the usefulness of the profile

Figures 9 and 10 are montage plots of the individual spectra from the C_{60}^+ and Ar^+ depth profiles. In figure 9 the spectra from the 10 kV C_{60}^+ profile show stable composition with depth and the ability to observe different chemistries at the surface and interface with the Si substrate. In contrast, the spectra from the 250 V Ar^+ profile in figure 10 show evidence of immediate and increasing chemical damage as a function of depth. It is for this reason that Ar^+ sputter depth profiling has historically not been applied to polymers and organics and that C_{60} cluster ion sources have been developed.

Since C_{60} provides the ability to depth profile through many organic or polymer films and provide the expected compositional information, it becomes possible to depth profile multilayer systems and identify the different layers. C_{60} profiling can also be used to study effects such as migration of additives and surface modification of organic and polymer films.

Polystyrene
10 kV C_{60}^+ Depth Profile

Polystyrene
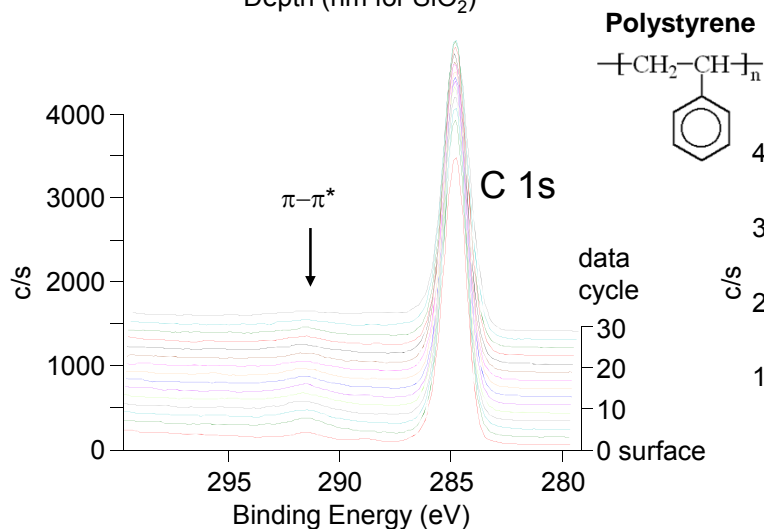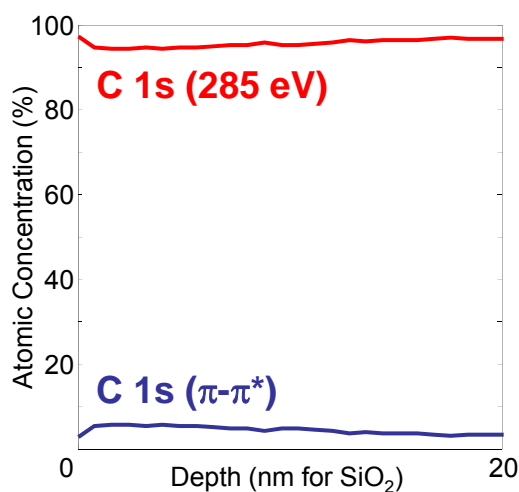## 250 V Ar^+ Depth Profile

Polystyrene

$-[CH_2-CH]_n-$

Figure 11. 10 kV C_{60}^+ depth profile into polystyrene and a montage plot of the C 1s spectra showing preservation of chemistry as indicated by the presence of the $\pi-\pi*$ peak as a function of depth.
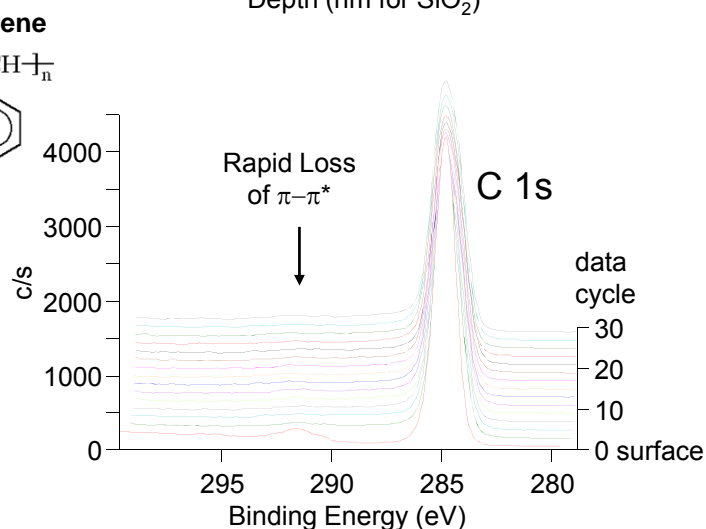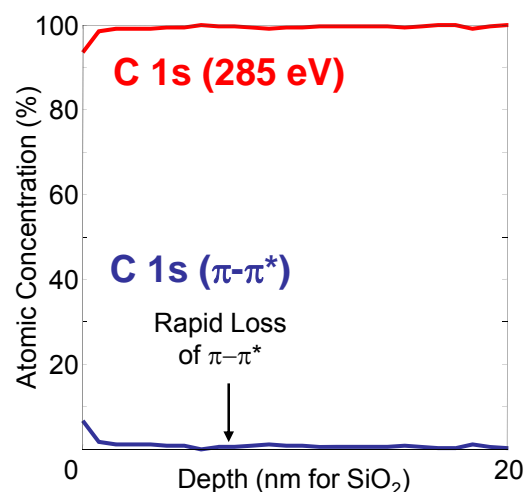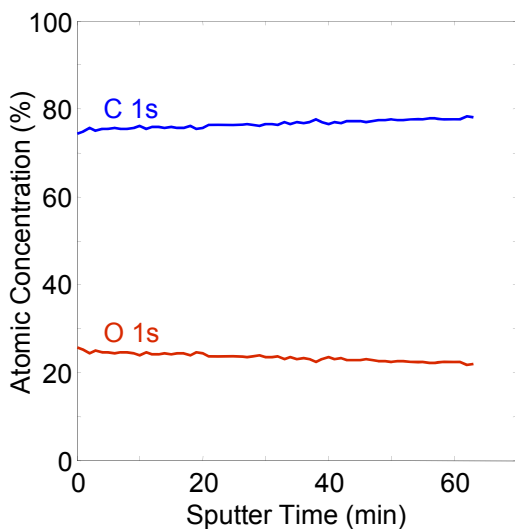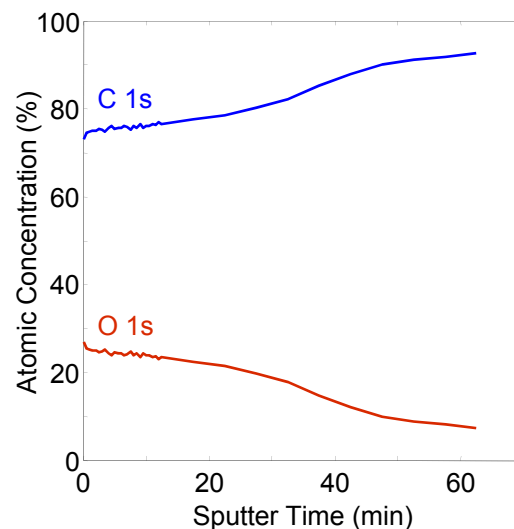
Figure 12. 250 V Ar^+ depth profile into polystyrene and a montage plot of the C 1s spectra show rapid chemical damage as indicated by the loss of the $\pi-\pi*$ peak.

Materials that contain aromatic structures or a high degree of cross linking can be challenging even for C_{60}. Results from these types of samples will be material dependent, but there are some basic observations that can be made. The sputtering efficiency will be reduced and the maximum depth that can be sputtered without chemical damage may be limited. Even though C_{60} may sputter these types of materials less efficiently, C_{60}^+ will typically do a better job of preserving chemistry than Ar^+. With Ar^+, one can expect rapid chemical damage that will be observed by the loss of peaks associated with C-O and N-O linkages.

The data in figures 11 and 12 show depth profiles and montage plots of the C 1s spectra obtained using 10 kV C_{60}^+ and 250 V Ar^+ to sputter into a polystyrene sheet to a depth of 20 nm (SiO_2 etch rate). This work was performed at room temperature. The C_{60} data shows the $\pi-\pi^*$ peak remains throughout the profile. In contrast the low voltage argon profile data shows an immediate and rapid loss of the $\pi-\pi^*$ peak indicating rapid damage to the aromatic structure of the polystyrene.
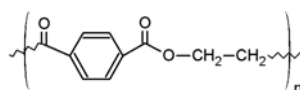
PET - 10 kV C_{60}^+ With Zalar Rotation

PET - 10 kV C_{60}^+ Without Zalar Rotation
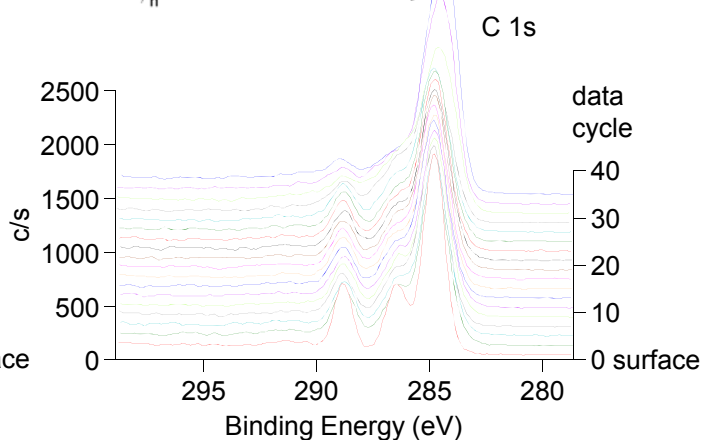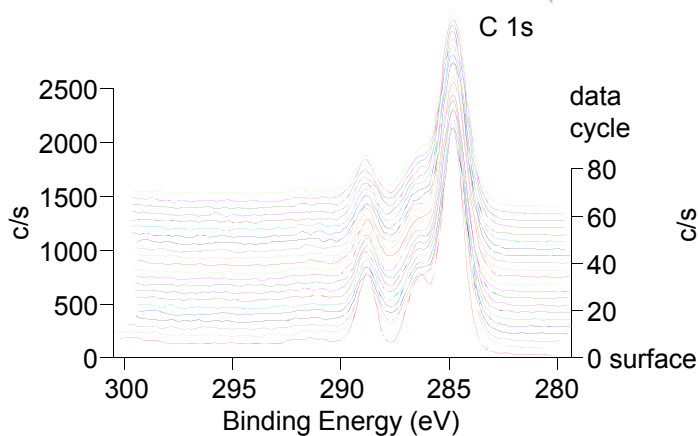
PET

Notice C growth

Figure 13. 10 kV C_{60}^+ sputter depth profile into a thick PET film with the use of Zalar rotation. For the conditions used approximately 100 nm would have been removed based on the etch rate for SiO_2. AFM measurements indicated 240 nm of PET was removed.

Figure 14. 10 kV C_{60}^+ sputter depth profile into a thick PET film without the use of Zalar rotation. The same sputtering conditions were used for the depth profiles shown in figures 13 and 14. Note the sudden change in surface composition beginning at T=30 min in this non-Zalar depth profile.

Zalar Rotation: It has been observed with XPS and TOF-SIMS C_{60} sputter depth profiling that there is a limit to how deep one can sputter without seeing a change in chemistry.[7] It has also been observed that Zalar (azimuthal) rotation can be used to extend the sputter depth where chemical composition is preserved.

To illustrate this phenomena a polyethylene terephthalate (PET) sheet was sputtered with a 10 kV C_{60} ion beam to an estimated depth of 240 nm into the PET (100 nm for SiO_2). This work was performed at room temperature.

PET - 10 kV C_{60}^+
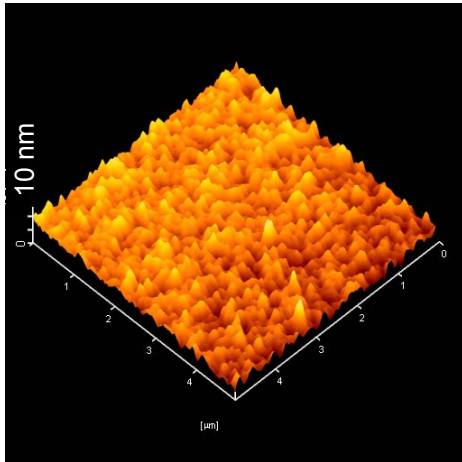# With Zalar Rotation

Figure 15. AFM image of the sputter crater bottom from the sample where Zalar rotation was used, showing a surface roughness of 10 nm.

Data from the depth profile collected with Zalar rotation is shown in figure 13. The sputter depth profile shows stable composition for the first 20 minutes followed by a slow increase in the C 1s peak intensity. The montage plot of the individual C 1s spectra shows characteristic PET spectra throughout the depth profile.

Data from the depth profile collected without Zalar rotation is shown in Figure 14. The sputter depth profile shows stable composition for the first 10 – 15 minutes followed by a transition to a carbon rich state. The montage plot of the individual C 1s spectra shows characteristic PET spectra during the period of stable composition at the beginning of the depth profile. During the transition period to the carbon rich state, the C 1s spectrum changes. The PET component of the spectrum is diminished and the C-C peak grows in intensity.

To explore what role surface roughening has in this situation, AFM images were collected from the bottom of the sputter craters and are shown in figures 15 and 16.

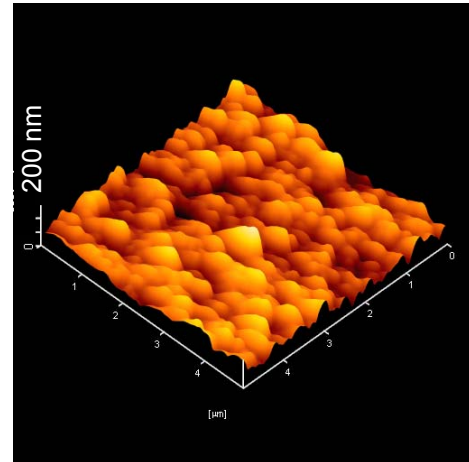# PET - 10 kV C_{60}^+
Without Zalar Rotation

Figure 16. AFM image of the sputter crater bottom from the sample where Zalar rotation was not used, showing a surface roughness of 200 nm.
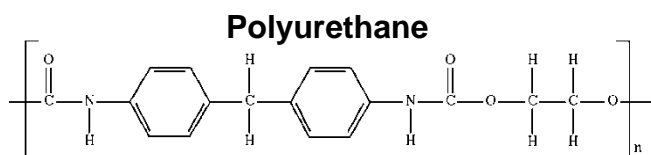
The AFM image obtained from the sample where Zalar rotation was used shows a surface roughness of 10 nm (figure 15). In contrast, the sample depth profiled without Zalar rotation has a surface roughness of approximately 200 nm (figure 16).

The conclusion we have drawn from the data shown in figures 13-16 is that as surface roughness increases, portions of the sample are shadowed from the ion beam and carbon from the C_{60} ion beam accumulates in these areas. However when Zalar rotation is used, the sputtered surface remains smoother as shown in figure 15. The smooth surface is sputtered more effectively and the expected composition is maintained to a greater depth.

Applications: The study of basic materials is of general interest to understand the capabilities and limitations of C_{60} sputtering. However, it is the demonstrated practical application of C_{60} depth profiling that has led to the installation of sixty *06-C60* ion guns in laboratories around the world.

Polymer Additive Migration: The data shown in figures 17 and 18 is from a processed polyurethane part that contains a wax additive. It was suspected that the wax additive was migrating to the surface of the part, but it was not possible to prove it using an Ar^+ sputter depth profile. However, a 10 kV C_{60}^+ depth profile showed the presence of a thin (15 nm) surface layer that was depleted in O and N (components of polyurethane). The C 1s spectra from the depth profile show a different peak shape (fingerprint) in the surface layer than is observed below the surface. The C 1s peak shape in the surface layer is consistent with the wax additive and the peak shape below the surface is consistent with polyurethane. Using the Linear Least Squares fitting routine in the PHI MultiPak data reduction software, these two peak shapes were selected as basis spectra and used to create the C 1s chemical depth profile shown in figure 17.

Several observations about the practical use of C_{60} depth profiling can be made from this example: First, it was possible to obtain chemical state information from the surface layer and remove it. Second, after removing the surface layer, the polymer material below it was exposed with its chemistry intact and it was possible to continue sputtering into the polymer with no loss of chemical state information. As a result, it was possible to determine the relative thickness of the surface layer and observe the distribution of the additive as a function of depth based upon its XPS chemical fingerprint.
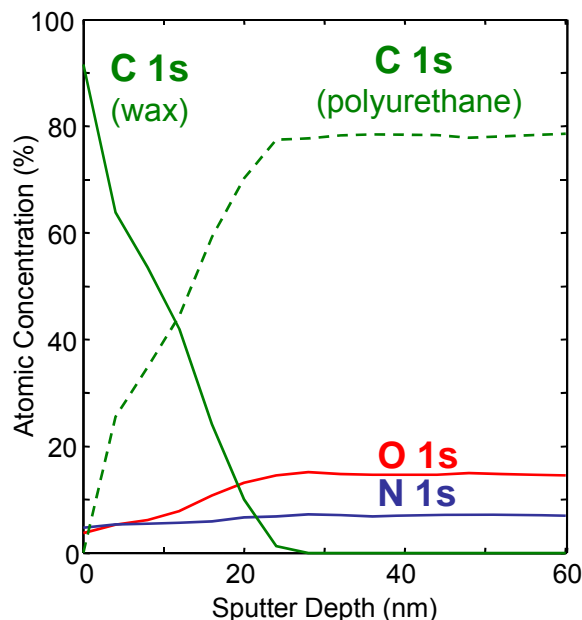
Polymer Additive Migration

Figure 17. 10 kV C_{60}^+ depth profile of a polyurethane part showing migration of a wax additive to the surface.
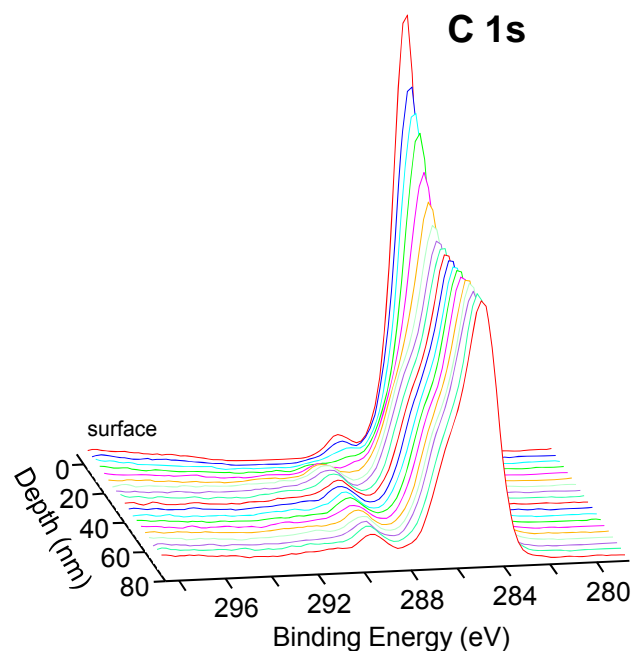

Figure 18. Montage plot of the C 1s spectra from the polyurethane profile shows the spectral shape for a wax near the surface and polyurethane below the surface.

Polyurethane

Drug Distribution in a Biomedical Coating:

The data shown in figures 19 and 20 is from a biomedical coating that is a 50/50 mixture of rapamycin and PLGA. The drug (rapamycin) is in a PLGA time release coating. The 10 kV C_{60}^+ depth profile shows that the rapamycin is segregated to the surface of the film. Below the surface film is a rapamycin depleted zone and finally the expected composition for the 50/50 mixture. The ability to see the location and distribution of the drug in the coating is very useful information for evaluating the coating process and determining how the coating will perform. The depth profile also shows the presence of Si at the surface.

The C 1s spectra in figure 20 show the surface to be depleted in PLGA (rich in rapamycin) followed by a PLGA rich zone and finally the expected mixture of PLGA and rapamycin.

Rapamycin
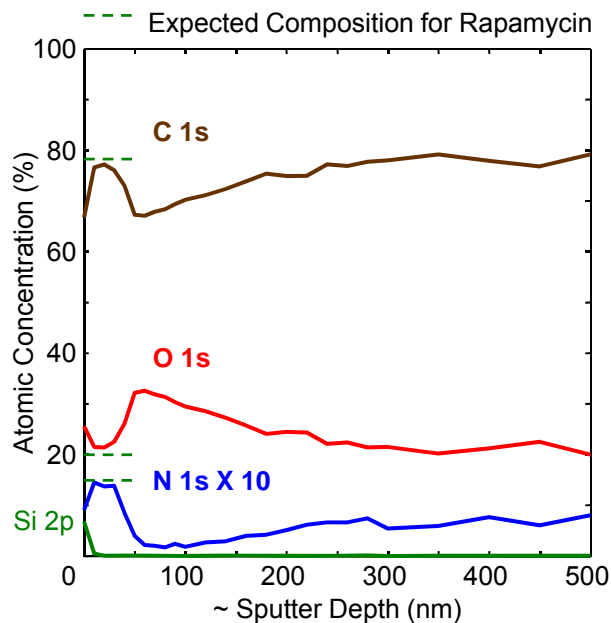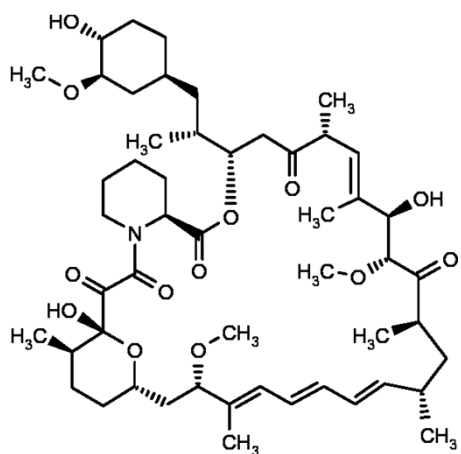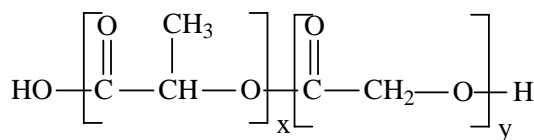
PLGA

Drug Distribution in a Biomedical Coating

Figure 19. 10 kV C_{60}^+ depth profile of a 50/50 rapamycin and PLGA film showing segregation of the rapamycin to the surface of the coating.
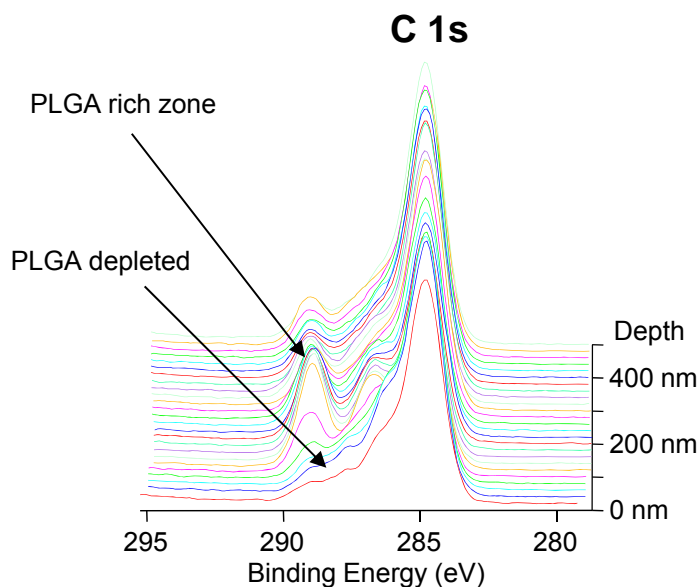
Figure 20. Montage plot of the C 1s spectra from the depth profile shows a rapamycin rich surface followed by a rapamycin depleted layer and finally the expected composition for the 50/50 mixture.

Organic OLED Films: The data shown in figures 21 and 22 is from a model hole transfer layer for OLED display applications. The layer is a mixture of PEDOT and PSS. The 10 kV C_{60}^+ depth profile suggests that near the interface with the ITO the film becomes rich in PEDOT.

The S 2p spectra shown in the montage plot in figure 22 show the presence of two chemical states for S. The higher binding energy peak is from the sulfone groups in the PSS and the lower binding energy peak is from the organic S in the PEDOT. From this data we can see that there is a mixture of the two components throughout the film and that the PEDOT is present at lower concentrations near the surface and higher concentrations near the bottom of the film. Previously presented work shows that the sulfone chemistry is damaged by Ar^+ sputtering making it difficult to correctly detect the distribution of PEDOT and PSS within the film if Ar^+ sputtering is used.
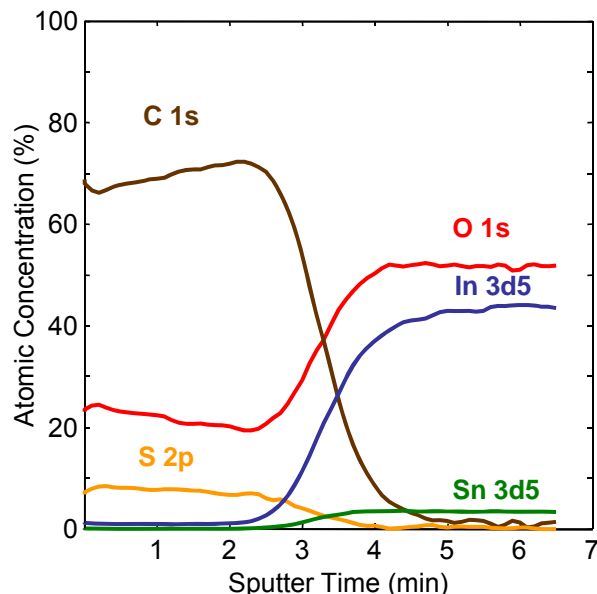
Organic OLED Films

Figure 21. 10 kV C_{60}^+ depth profile of a hole transfer layer for an Organic LED (OLED) device.

Poly(styrenesulfonate)

PSS

PEDOT

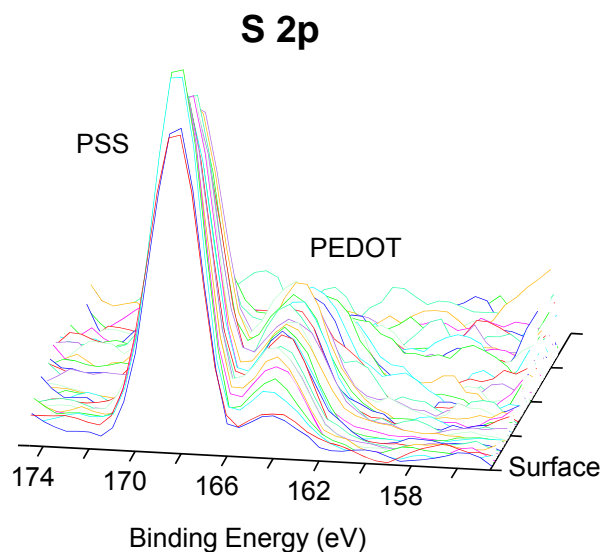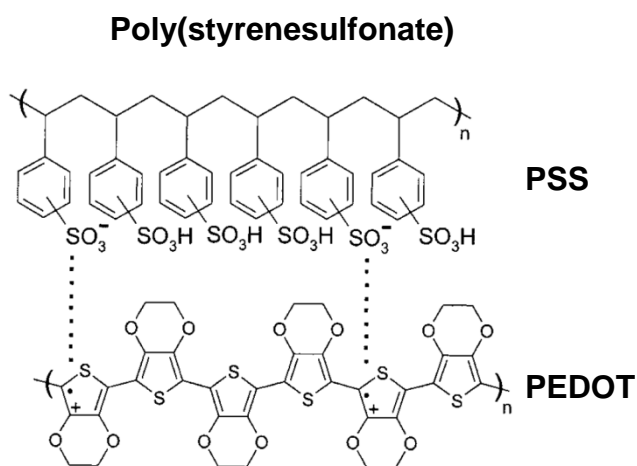**Poly(3,4-ethylenedioxythiophene)**

S 2p

Figure 22. Montage plot of the S 2p spectra from the depth profile showing preservation of the fragile sulfone chemistry associated with the PSS component of the layer.

PHI *06-C60*: The PHI model *06-C60* ion gun is uniquely designed for sputter cleaning and sputter depth profiling of organic and polymer materials. The C_{60} ion beam and instrument geometry provide this capability with efficient etch rates and low sample damage rates for many materials. The *06-C60* is an optional accessory for current PHI XPS and TOF-SIMS instruments.

Figure 23. PHI model 06-C60 sputter ion gun.

06-C60 Specifications	
Beam Voltage	1 – 10 KV
Maximum Beam Current Long Life Mode	20 nA @ 10 kV
Minimum Beam Diameter	< 1 mm*
Maximum Beam Deflection	10 x 10 mm*
C_{60} Source	Heated Reservoir
Ionization Method	Electron Impact
Working Distance	50 – 63 mm

* at 63 mm working distance

Figure 24. Schematic diagram of the PHI model 06-C60 sputter ion gun.

References:

1. N. Sanada, A. Yamamoto, R, Oiwa, Y. Ohashi, *Surface and Interface Analysis*, 36 (3), (2004) 280-282.

2. K. Tanaka, N. Sanada, M. Hikita, T. Nakamura, T. Kajiyama, A. Takahara, *Applied Surface Science*, 254, (2008) 5435-5438.

3. Y. Chen, B. Yu, W. Wang, M. Hsu, W. Lin, Y. Lin, J. Jou, J. Shyue, *Analytical Chemistry*, 80, (2008) 501-505.

4. Z. Postawa, B. Czerwinski, M. Szewczyk, E. J. Smiley, N. Winograd and B. J. Garrison, *Analytical Chemistry*, 75, (2003) 4402-4407.

5. T. Miyama, N. Sanada, S. Ida, J. Hammond, M. Suzuki, *Applied Surface Science*, 255 (2008) 951-953.

6. T. Nobuta & T. Ogawa, *Journal of Materials Science*, 44, (2009) 1800-1812.

7. G. Fisher, M. Dickinson, S. Bryan, J. Moulder, *Applied Surface Science*, 255 (2008) 819-823.